Self-Association of Enolase from *Trichomonas vaginalis*. Monomers, Dimers, and Octamers Coexist in Solution

Elibeth Mirasol-Meléndez,[†] Enrique Lima,[‡] Victor Lara,[§] Luis G. Brieba,[∥] Samuel Lara-González,[⊥] and Claudia G. Benitez-Cardoza*,[†]

[†]Laboratorio de Investigación Bioquímica, Escuela Nacional de Medicina y Homeopatía-Instituto Politécnico Nacional, Guillermo Massieu Helguera No. 239, La Escalera Ticoman, CP 07320 Ciudad de Mexico, Mexico

[‡]Instituto de Investigaciones en Materiales, Universidad Nacional Autónoma de Mexico, Circuito exterior s/n, Cd. Universitaria, Del. Coyoacán, CP 04510 Ciudad de Mexico, Mexico

[§]Universidad Autónoma Metropolitana, Iztapalapa, Av. San Rafael Atlixco No. 186, Col. Vicentina, 09340 Ciudad de Mexico, Mexico

[∥]Laboratorio Nacional de Genómica para la Biodiversidad, Centro de Investigación y de Estudios Avanzados del IPN, Apartado Postal 629, Irapuato, CP 36821 Guanajuato, Mexico

[⊥]División de Biología Molecular, IPICYT, Camino a la Presa San José 2055, CP 78216 San Luis Potosí, San Luis Potosí, Mexico

S *Supporting Information*

ABSTRACT: We used small-angle X-ray scattering to study the self-association of enolase from *Trichomonas vaginalis* as a function of the protein concentration and cosolute type. We observed coexisting monomers, dimers, and octamers in variable relative populations, depending on whether Tris−acetate, Tris−HCl, or potassium phosphate buffers were used. Phosphate ions hindered the formation of dimers and octamers. In contrast, the populations of dimers and octamers increased in Tris−acetate or Tris−HCl buffers and additionally increased by augmenting protein concentration or adding magnesium. Single oligomeric species could not be isolated in any of the experimental conditions tested. Furthermore, the secondary and tertiary structures, as well as the temperature-induced denaturation of the mixtures of species, were investigated. The acquired species lost enzymatic activity, but they were prone to interact with plasminogen, as judged from changes in the secondary and tertiary structures upon complex formation.
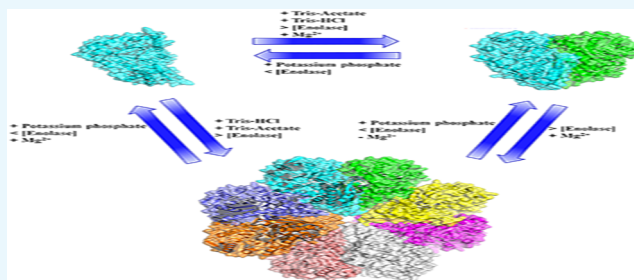
INTRODUCTION

Enolase is a moonlighting protein that performs a variety of functions. Its canonical task is catalyzing the reversible dehydration of 2-phosphoglycerate (2-PGA) to phosphoenolpyruvate (PEP) in glycolysis and gluconeogenesis. For catalysis, Mg^{2+} is the main physiological cofactor of enolase and promotes its highest activity but some other metals, such as Mn^{2+} and Zn^{2+}, can also bind and activate the enzyme.[1] Enolase is also involved in cellular stress; bacterial, parasitic, and fungal infections; and autoantigen activities, as well as the occurrence and metastasis of cancer and the growth, development, and reproduction of organisms.[2] Markedly, the surface localization of enolase has been shown for several cell types, including bacteria, fungi, protozoans, and mammals, serving to recruit and promote plasminogen activation pericellularly and contributing to immune evasion and tissue invasion processes.[3−6]

Structurally, enolase is typically a homodimeric protein in which each monomer has a large domain (C-terminal) with an $\alpha\alpha\beta\beta$ $(\alpha/\beta)_6$ barrel folding type and a small domain (N-terminal) with three α-helices and four β-strands. The active site is located at one end of the barrel, but both domains include loops that fold over the active site when the substrate is bound.[7−10] Subunit contacts for homodimer formation are between the small domain of one subunit and the large domain of the other. In addition, the crystal structure of enolase from some species, such as *Staphylococcus aureus*, *Streptococcus pneumoniae*, *Streptococcus suis*, and *Bacillus subtilis*, has revealed octameric arrangements,[10−13] which are described as wheel-shaped scaffolds formed from a tetramer of dimers.[14] In octamers, the overall scaffolds of monomers and dimers are quite similar to those of dimeric enolases. The octameric structure holds two types of oligomerization interfaces opposite to each other: one holds the two monomers together (to form dimers), and the other corresponds to neighboring dimers (to form octamers).[15]

Trichomonas vaginalis is a protist that causes the most common nonviral sexually transmitted infection in humans,

known as trichomoniasis.[16] In the *T. vaginalis* sequence database,[17] there are nine genes annotated as enolase, even though at least two of them should be incapable of performing enzymatic activity since they lack the active-site amino acid residues. Furthermore, the product of the gene encoded by TVAG_329460 (UniProt entry A2EBB4) was described as an anchorless, surface-associated plasminogen receptor in *T. vaginalis*.[18] In addition, enolases from *T. vaginalis* show two distinctive characteristics from the enolase of the human host. One characteristic corresponds to three key substitutions within one of the loops of the active site compared with host enolase. The other characteristic is a unique N-terminal motif, composed of 15−18 residues, on all potentially active enolases, whose function still must be established. These features have positioned enolase as an important cell-surface virulence factor and as a potential drug and vaccine target as well as a diagnostic marker to fight trichomoniasis.[19]

The crystallographic structure has not been solved for any of the enolases from *T. vaginalis*, and the oligomeric state of them is yet to be analyzed. Therefore, we studied the oligomeric state of enolase from *T. vaginalis* (TvEno) in a variety of experimental conditions. We found that monomers, dimers, and octamers coincide in solution and their populations depend on the cosolute and protein concentrations. The secondary structure and tryptophan environment as well as thermal unfolding transitions of enolase solutions were studied by circular dichroism (CD) and fluorescence spectroscopies.

Enolase is a moonlighting protein, which participates in multiple biochemical processes, apart from enzymatic activity, in several cellular locations. This means that enolase is submitted to a variety of physicochemical environments. One of the most studied nonenzymatic functions of enolase is binding of plasminogen on the cell surface of several organisms. Some reports indicate that non-native structures (monomers and multimers) of *Streptococcus pyogenes* (Sp) enolase are capable of interacting with canine plasminogen. On the contrary, when Sp enolase and plasminogen are soluble, correctly and completely folded, and in the case of enolase, fully active, no binding occurs.[55] Therefore, a bunch of questions arise; for example, what gives enolase its functional plasticity? What is the conformation or oligomeric state that performs each of the jobs of enolase? How enolase is targeted to multiple cellular locations? What determines the specificity of enolase for each of its ligands? Since information about the structure of the enolase under the various experimental conditions is lacking, we were curious to investigate the oligomeric state, secondary and tertiary structures, and stability of enolase in a variety of physicochemical conditions, particularly where enolase does not show enzymatic activity. Indeed, these conditions are not identical to those found in the cellular environment but our results shed light on the conformational and oligomeric-state changes that enolase can undergo in performing a variety of functions, particularly plasminogen binding.

■ RESULTS

Purification and Enzymatic Characterization. All enolases from *T. vaginalis* have a unique N-terminal extension of 34−63 amino acid residues, which is absent in enolases from other organisms.[19] In this work, an N-terminal truncated version of enolase, eliminating 34 amino acid residues (TvEnoΔ34), was used in all experiments. This construct is similar in the number of amino acid residues in enolases from

other biological species. The recombinant His-tag-cleaved enolase protein was successfully purified, producing yields of approximately 7.5−10 mg of protein per liter of culture. Kinetic characterization of the TvEnoΔ34 enolase construct was successfully achieved in triethanolamine (TEA) buffer. The kinetic parameters determined are as follows: specific activity of 212.36 μmol min^{-1} mg^{-1} of enzyme, a turnover (k_{cat}) of 3.53 s^{-1}, and a K_M equal to 5.17 nM. Several attempts to measure the enzymatic activity in Tris−HCl, Tris−acetate, or potassium phosphate buffers were made under a variety of experimental conditions (different temperatures were tested as well as concentration of reactants). Nevertheless, we could not detect the conversion of the substrate 2-PGA into the product PEP when buffers different from TEA were used. Conversely, enzymatic activity was detectable in positive control assays, using enolase from *Saccharomyces cerevisiae*, in Tris−acetate and Tris−HCl buffers, with similar specific activity as in TEA buffer (110 μmol min^{-1} mg^{-1} of enzyme). As discussed below, slight conformational changes (involving secondary and tertiary structures) might have occurred to enolase from *T. vaginalis* when it was diluted in Tris−acetate and in Tris−HCl buffers. Consequently, the fine arrangement of amino acid residues and loops within the catalytic site on the protozoan enzyme was altered. Regarding the phosphate ions, they are a well-known competitive inhibitor of enolase.[1] As expected, we could not detect enzymatic conversion for either TvEnoΔ34 or enolase from yeast.

Oligomeric State of Enolase Solutions. Small-angle X-ray scattering (SAXS) is useful for determining the oligomeric states and quaternary structures of proteins in solution.[28] The SAXS Kratky profiles (Figure S1) allowed us to determine the size and shape of enolase solutions under a variety of experimental conditions. The size distributions obtained are summarized in Figure 1. In most buffers, at least two protein
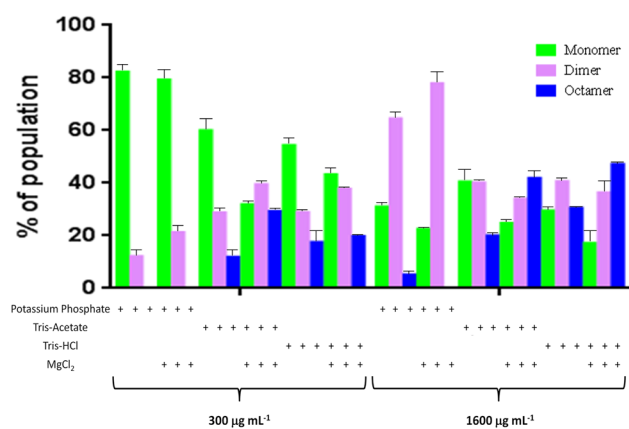
Figure 1. Percentage of population of each oligomeric state of TvEnoΔ34 from *T. vaginalis* in different buffer conditions. SAXS experiments were performed using two different protein concentrations (300 and 1600 μg mL^{-1}, as indicated). The buffer solution in which enolase was diluted is indicated with crosses at the bottom of the figure.

concentrations were evaluated (300 and 1600 μg mL^{-1}) and in some cases, protein solutions at 30 μg mL^{-1} were also tested. The most remarkable feature of this data is that monomers, dimers, and octamers could be detected in equilibrium, in most of the experimental conditions, depending on the protein concentration and the nature of the cosolute. In all conditions
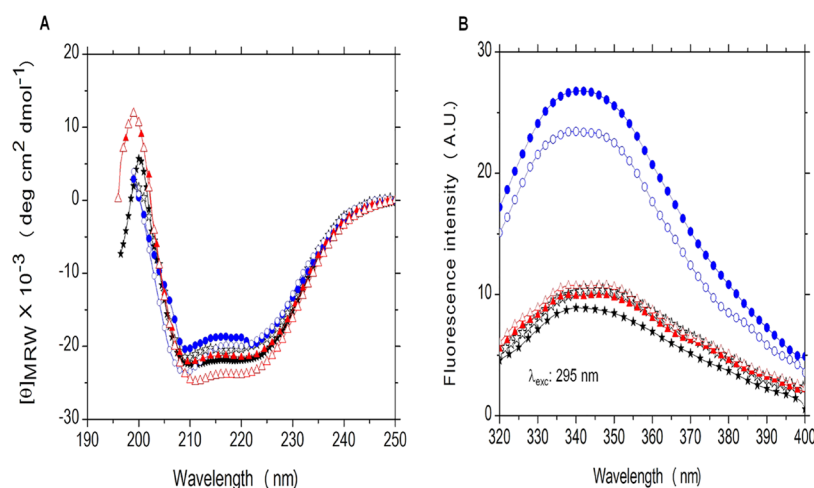
Figure 2. (A) Far-UV circular dichroism and (B) intrinsic fluorescence-emission (excitation wavelength 295 nm) spectra of native recombinant TvEnoΔ34. Enolase was diluted in Tris−HCl buffer (solid stars), Tris−HCl buffer complemented MgCl₂ (open stars), Tris−acetate buffer (solid circles), Tris−acetate buffer plus MgCl₂ (open circles), potassium phosphate buffer (solid triangles), and potassium phosphate buffer with MgCl₂ (open triangles). All spectra were obtained at 25 °C and pH 8.0. The final concentration of MgCl₂ was 2 mM.

tested, it was not possible to obtain monodisperse systems, with a single species populated, even by varying protein concentrations by more than 50-fold.

Additionally, some attempts to isolate a single oligomeric-state species by gel-filtration chromatography were made (Agilent Bio SEC-5, HPLC column, 0.2 mL min⁻¹; data not shown) but equilibria were rapidly restored, according to protein concentration and cosolute. In the following paragraphs, we describe the results obtained in each buffer solution.

Potassium Phosphate Buffer. The highest proportion of monomers was detected in potassium phosphate buffer at 30 (data not shown) and 300 μg mL⁻¹ either in the absence or presence of Mg²⁺ (≈82 and 79%, for apo- and holo-enolase, respectively). When the protein concentration was increased up to 1600 μg mL⁻¹, using this buffer, the percentage of dimers increased (64.3 and 77.7% for apo- and holo-enolase, respectively). Interestingly, only a small amount of octamers could be detected but only in the case of apo-enolase (6.1 and 4.9% at 300 and 1600 μg mL⁻¹, respectively; octamers were not detected at the lowest protein concentration of 30 μg mL⁻¹) since octamers could not be observed when the divalent cofactor was added to the protein solution.

Tris−HCl Buffer. As expected, the oligomerization state was highly dependent on the protein concentration. In this buffer solution, the monomer dominated at a low protein concentration (300 μg mL⁻¹) for both apo- (54.1%) and holo-enolase (43%). Under these conditions, the dimer constituted 28.6 and 37.5% of the protein solution in the absence and presence of Mg²⁺, respectively. The octamer accounted for 17.3 and 19.5% for apo- and holo-enolase, respectively. When the protein concentration was increased to 1600 μg mL⁻¹ in Tris−HCl buffer, monomers were less abundant and the concentration of dimers and octamers increased. For apo-enolase, at 1600 μg mL⁻¹, monomers and octamers were almost equally populated (≈30% of each species) whereas the population of the dimer accounted for approximately 40%. In the case of holo-enolase, the octamer was even more favored (46.9%; the highest concentration of octamers obtained in all conditions tested) whereas the population of monomers dropped to 16.9% and the dimer was slightly increased to 36.2%.

Tris−Acetate Buffer. At low protein concentrations (300 μg mL⁻¹), monomers were favored for apo-enolase (59.8%), followed by dimers (28.5%), whereas octamers represented 11.7% of the population of this solution. When the divalent cofactor was added to the solution while maintaining the protein concentration, dimers were favored (39.3%), followed by monomers in which the concentration dropped to 31.7% and the octamer population increased to 29%.

At high protein concentrations of apo-enolase (1600 μg mL⁻¹), monomers and dimers were almost equally populated (≈40%) whereas octamers represented approximately 20% of the species. At this protein concentration, for holo-enolase, the highest order oligomeric state was preferred (41.7%). In this case, the monomer and dimer populations were 24.5 and 33.8%, respectively.

Secondary and Tertiary Structures of Monomer−Dimer−Octamer Mixtures. The secondary structure and hydrophobic environment of tryptophanyl residues of the mixtures with variable populations of monomer−dimer−octamer were assessed by circular dichroism and intrinsic fluorescence spectroscopies. Since all solutions studied represent at least two different oligomeric states, the CD and fluorescence signals are the contribution of all species present in each solution, according to their relative populations.

In Figure 2, the CD and intrinsic fluorescence-emission spectra of apo- and holo-enolase at three different buffer conditions, 50 mM potassium phosphate, 50 mM Tris−acetate, and 50 mM Tris−HCl, at pH 8 are shown. In all cases, the concentration of MgCl₂ was 2 mM (although other concentrations of MgCl₂ were also evaluated, the data are not shown). All CD spectra were not identical but quite similar, showing the characteristic shape of an α/β protein, with two negative peaks centered at approximately 220 and 208 nm. The largest CD signal intensity was observed for enolase diluted in potassium phosphate buffer, complemented with Mg²⁺, the buffer condition where the relative population of monomers was close to 80%, dimers represented approximately 20% of the total protein, and octamers were nearly absent. CD spectra obtained in other buffer conditions showed that the helical content of enolase might decrease while increasing the β-sheet content. Considering the relative populations of monomers,
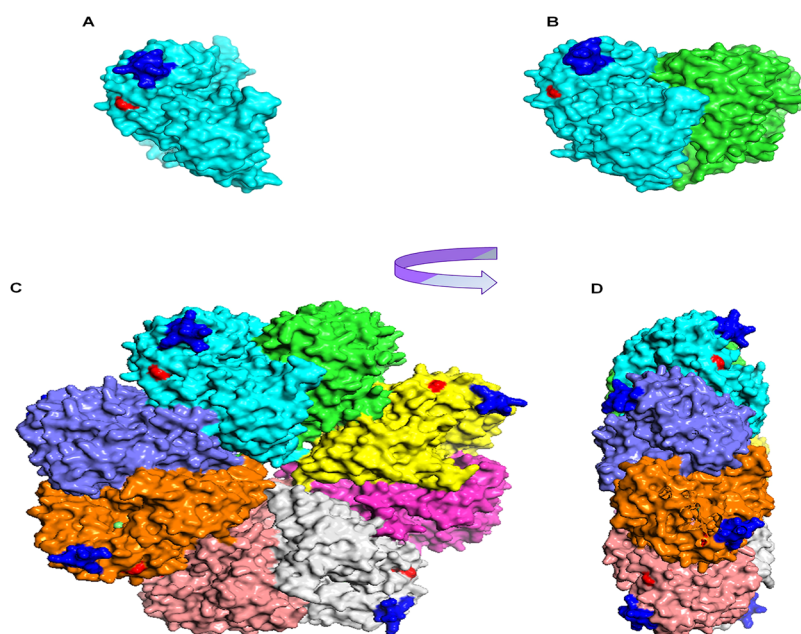
Figure 3. Three-dimensional models of monomers, dimers, and octamers of TvEnoΔ34. The subunits of each structure are colored for clarity. In each panel, Trp314 and 348 are represented in red. The putative plasminogen-binding site is shown in blue. (A) Monomer, (B) dimer, and (C, D) octamer.

dimers, and octamers in each buffer condition, it appears that an increase in dimer concentration and/or formation of the octameric species led to a slight decrease in helical content with a concomitant increase in β-sheet content.

Markedly, the effect on the secondary structure of the divalent cation was different in each buffer solution. In Tris−HCl buffer complemented with 2 mM $MgCl_2$ (where dimers and octamers were increased in relative population), TvEnoΔ34 showed less helical content than in the absence of the cofactor. In contrast, when Tris−acetate buffer was complemented with the same $MgCl_2$ concentration and concomitantly, dimers and octamers were favored with respect to monomers, enolase gained helical structure (Figure 2). This means that different cosolutes apart from leading to different combinations of oligomeric species might also induce slightly different conformations of these species.

Intrinsic fluorescence-emission spectra (λ_{exc} = 295 nm) are shown in Figure 2. The values of the corresponding spectral center of mass (SCM) are shown in Figure S2. These values varied between 352 and 355 nm depending on the buffer solution used. The shortest SCM value (352 nm) was observed for holo-enolase in Tris−acetate buffer, whereas the largest SCM observed corresponded to holo-enolase diluted in Tris−HCl buffer. Furthermore, fluorescence spectra showed different emission intensities; the highest fluorescence-emission intensities were detected for enolase diluted in Tris−HCl buffer, either in the absence or presence of $MgCl_2$. TvEnoΔ34 showed a similar fluorescence-emission intensity when it was diluted either in Tris−acetate buffer or potassium phosphate buffer. The main differences between these spectra were the positions of the SCM.

These results confirm slight variations in the conformation of enolase from *T. vaginalis* when changing buffer solutions. In Figure 3, the three-dimensional (3D) models corresponding to monomeric, dimeric, and octameric TvEno are shown. In the three models, the structures of monomers are almost superimposable, except for some displacements of loops and

markedly of helix α1 situated at the dimer−dimer interface when the octamer is formed. Additionally, β-strand 3, at the monomer−monomer interface seems to be shorter (adopting a more relaxed conformation) in the monomer than in the dimer or the octamer.

Regarding tryptophan residues, the sequence of TvEno has two of these, which are situated in helix α10 (Trp314) and in the loop α11 and β-strand 11 (Trp348). They appear as close neighbors in the three-dimensional structure. Since Trp348 is in a loop, it might have higher mobility and exposure to the solvent than Trp314. Unpublished data from our lab obtained by molecular dynamics simulation of monomeric enolase confirm that the side chain of Trp348 might have a larger tendency to be exposed to solvent than Trp314. Neither Trp314 nor Trp348 are near the interfaces (monomer−monomer or dimer−dimer). Therefore, these residues cannot participate in interface formation. This means that changes in the SCM of the fluorescence-emission spectra of TvEnoΔ34 due to modification of the buffer solution were a consequence of conformational adaptations within each monomer when forming different oligomeric-state species.

Thermal Stability of Monomer−Dimer−Octamer Mixtures. The thermal denaturation of *T. vaginalis* enolase solutions was assessed by recording the temperature-induced denaturation profiles in potassium phosphate, Tris−HCl, or Tris−acetate buffers. The transitions were followed by monitoring the ellipticity at 220 nm, with constant heating rates (2 °C min^{-1}), as shown in Figure 4. We observed that transitions obtained in Tris−acetate buffers without Mg^{2+} appear as single sigmoid curves, whereas the transition in Tris−HCl buffer without Mg^{2+} appeared as a very broad, complex sigmoid curve, indicating the presence of several steps between 35 and 85 °C. The profile obtained in potassium phosphate buffer shows an interesting characteristic. The secondary structure of apo- and holo-enolase was not significantly altered by thermal treatment in potassium phosphate buffer conditions, as judged from the CD signal,
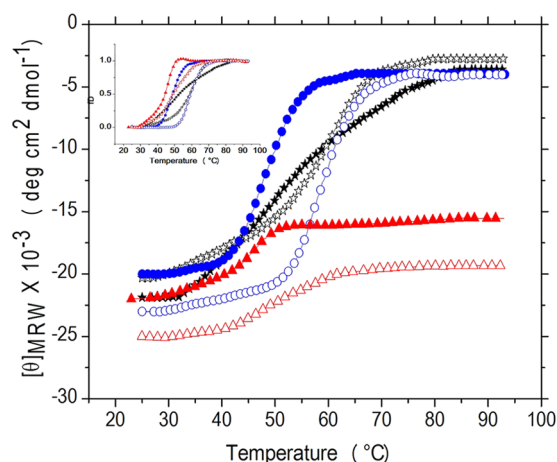
Figure 4. Temperature-induced thermal denaturation profiles of enolase TvEnoΔ34 monitored by CD spectroscopy in Tris−HCl buffer (solid stars), Tris−HCl buffer plus MgCl₂ (open stars), Tris−acetate buffer (solid circles), Tris−acetate buffer complemented with MgCl₂ (open circles), potassium phosphate buffer (solid triangles), and potassium phosphate buffer complemented MgCl₂ (open triangles). The denaturation process was followed by recording ellipticity at 220 nm. The inset shows normalized data. The final concentration of MgCl₂ was 2 mM.

which was reduced by approximately 5 units (θ_{MRW}), whereas profiles obtained in other buffer solutions had a reduction of the signal of approximately 15−18 units (θ_{MRW}). This means that the unfolded state obtained in potassium phosphate buffer retained a considerable amount of secondary structure and might be more compact, compared with the unfolded state achieved in the other two buffer solutions (either for apo- or holo-enolase).

When protein solutions were complemented with MgCl₂ (2 mM), the thermal denaturation process occurred at higher temperatures compared to those for protein solutions without MgCl₂ (Figure 4). This was more easily noticeable when the transitions were normalized (Figure 3 inset). This means that the divalent cofactor stabilized enolase from *T. vaginalis*, as observed for enolase from other biological species[29] as well as other enzymes that are stabilized by their cofactors.[30,31] In the case of TvEno, subunit interactions necessary to increase the percentage of dimers and oligomers as observed in Tris−HCl and Tris−acetate buffers upon cofactor binding might have contributed to the observed thermal stabilization (Figure 4). Commonly, from thermal denaturation profiles, it is possible to obtain thermodynamic parameters associated with the unfolding or refolding reaction when a denaturation model can be assumed to describe the experimental data. In this case, as stated before, enolase solutions were mixtures of oligomeric species; therefore, it was not possible to establish a denaturation model that can adequately describe the profiles.

Interaction with Plasminogen. CD is a widely used method to determine the secondary structure of proteins in solution. It, thus, can be used to determine whether there are changes in protein conformation when proteins interact with each other.[32−34]

The possible binding of plasminogen to the mixtures of TvEnoΔ34 and the conformational changes associated with this binding were analyzed using intrinsic fluorescence and far-UV CD. The spectra were recorded for each isolated protein and for both proteins in combination and are shown in Figure

5. In the same figure, the subtraction of the spectra is the spectra of the combined proteins minus the spectra of each protein recorded individually. In this case, four possible scenarios can be observed. The simplest one is that the TvEnoΔ34 mixture does not interact with plasminogen; therefore, CD and fluorescence spectra should remain unaltered and the spectra of the combination (plasminogen + TvEnoΔ34) must be equivalent to the algebraic addition of the spectra recorded for each of the proteins. A second possibility is that plasminogen and TvEnoΔ34 do interact, but this interaction does not modify the secondary or tertiary structures of either of the proteins involved. In this case, the complex formations should be transparent to CD and fluorescence spectroscopies. This case would not be distinguishable from the first scenario. Another option is that the interaction of plasminogen and TvEnoΔ34 occurs while altering the secondary and/or tertiary structure of only one of the proteins. In that case, the CD and/or fluorescence spectra would be different only for one of the proteins, with appreciable changes in the spectroscopic signals of the other protein upon complex formation. The last scenario would imply complex formation with concomitant conformational changes in both proteins that are appreciable in the CD and/or emission fluorescence signals.

Figure 5 shows a series of CD and fluorescence-emission spectra of TvEnoΔ34 and plasminogen in each of the buffers studied here in the absence and presence of MgCl₂. The results are also described for each buffer. It is important to mention that the plasminogen-binding site of enolase from *S. pneumoniae* is currently the best characterized. Two sites have been set; one of them is known as the C-terminal site and is composed of two lysine residues (433KK434) at the C-terminus. This site is nonconserved in enolases from *T. vaginalis* and in several confirmed plasminogen-binding enolases from several biological species. The internal site is composed of a nine-residue sequence motif (248FYDKERKVY256). Considering the sequence and structural alignments of enolases from *S. pneumoniae* and the product of gene TVAG_329460, the putative plasminogen-binding motif in TvEnoΔ34 corresponds to 264FYDEEKKLY272 (Figures 3 and S3).

Tris−HCl Buffer. In the absence of a divalent cofactor, there were no significant changes in the secondary structure upon combining plasminogen and TvEnoΔ34 since the CD signal of the mixture was almost equivalent to the addition of the spectra of each protein recorded separately. In contrast, the fluorescence signal of enolase was importantly quenched by the addition of plasminogen. The emission of the plasminogen was slightly quenched due to interaction with TvEnoΔ34. It is important to note that both tryptophan residues in TvEnoΔ34 are close to the putative plasminogen-binding site, so it is plausible that the interaction of enolase with plasminogen would modify the hydrophobic environment of the tryptophans.

When Mg²⁺ was added to this solution, we observed changes in the secondary structure of both enolase and plasminogen. The fluorescence signal of enolase was completely quenched. Since the addition of divalent cofactor implies an increment in dimer (mainly) and octamer concentrations, it implies that enolase might have a higher affinity toward plasminogen, as judged for larger changes in both spectroscopic signals, compared to that the solution without Mg²⁺. Notably, not only was enolase modified in its secondary and tertiary structures but also plasminogen adopted a different secondary
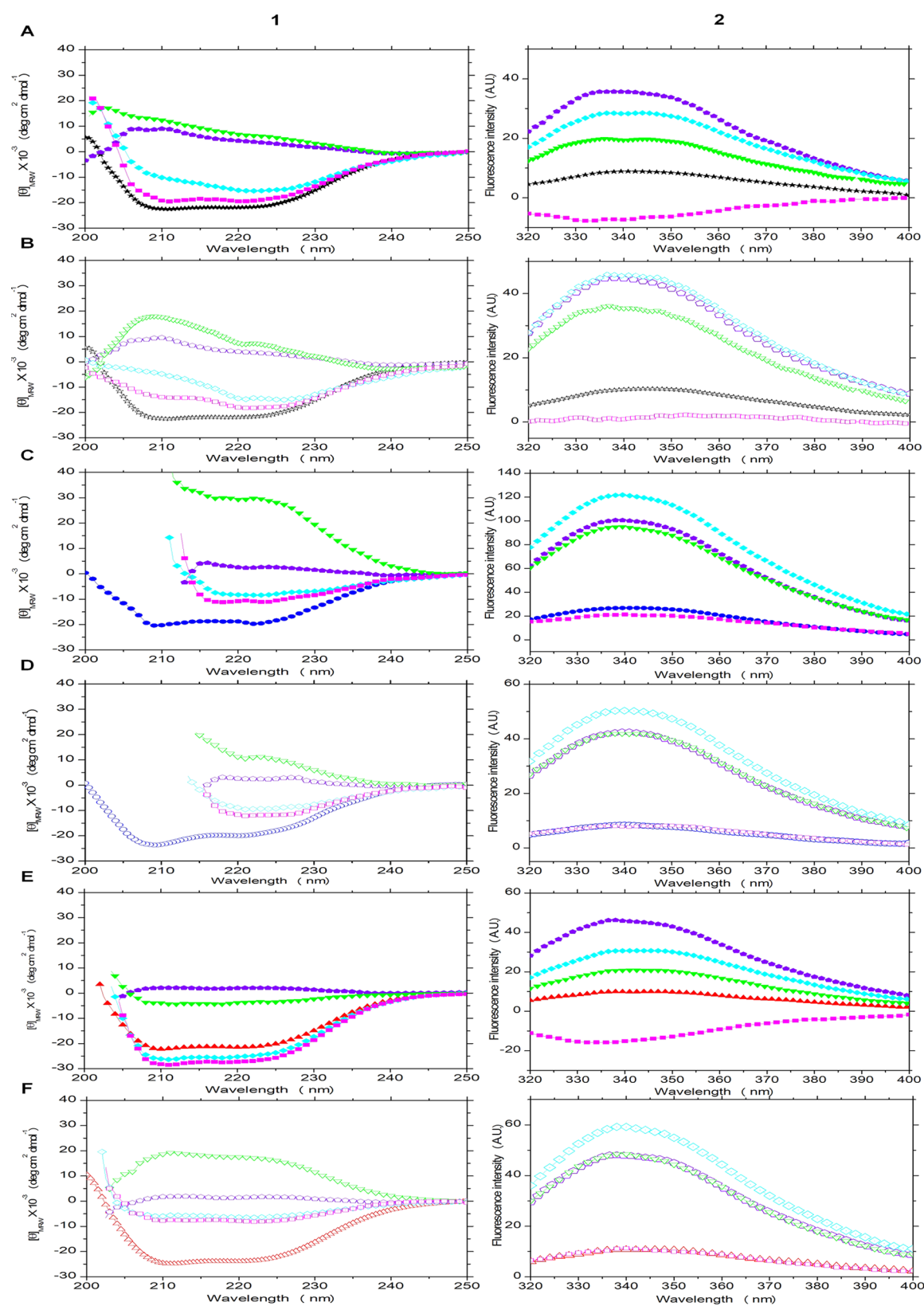
Figure 5. CD (1) and fluorescence-emission (2) spectra of different mixtures of enolase TvEnoΔ34 complexed with human plasminogen. Experiments were performed in native conditions at 25 °C and pH 8 in (A1, A2) Tris−HCl buffer; (B1, B2) Tris−HCl buffer complemented with $MgCl_2$; (C1, C2) Tris−acetate buffer; (D1, D2) Tris−acetate buffer with $MgCl_2$; (E1, E2) potassium phosphate buffer; and (F1, F2) potassium phosphate buffer plus $MgCl_2$. Samples are represented as follows: enolase (black stars, blue circles, and red triangles), plasminogen (violet pentagons), and enolase−plasminogen complex (cyan rhombus). The subtraction of the spectra corresponds to the spectra of the complex minus the corresponding spectra of native enolase (green triangles) or minus the spectra of plasminogen (magenta squares), which are also shown. Samples enriched with 2 mM $MgCl_2$ are represented with open symbols.

structure, as judged from the CD signal recorded in the absence and presence of Mg^{2+} in this buffer solution.

Tris–Acetate Buffer. In this buffer solution, either in the presence or absence of the divalent cofactor, we observed CD signal changes in both proteins but changes in plasminogen were more relevant. It seems that when the complex was formed, plasminogen gained secondary structure, whereas enolase lost it. Regarding the fluorescence-emission spectra, in both cases, the spectra of the combination corresponded merely to the addition of the individual contribution of the spectrum of each isolated protein. This means that despite important changes in the secondary structure of each protein upon interaction, they do not involve important changes in the hydrophobic environment of tryptophans. The changes in the spectra were similar in both conditions (with and without Mg^{2+}) but were more prominent in the absence of the cofactor.

Potassium Phosphate Buffer. In this solution, in the absence of MgCl$_2$, enolase gained secondary structure (α-helical content) upon complex formation, whereas the shape of the CD spectrum of plasminogen implied a transition between two random coil arrangements. Additionally, the fluorescence emission of both proteins was quenched upon interaction.

When the potassium phosphate buffer solution was complemented with Mg^{2+} and concomitantly, the percentage of dimers was raised from 11 to 20% and there was no population of detectable octamers, enolase lost an important amount of regular secondary structure whereas the CD signal of plasminogen indicated important changes in its secondary structure due to complex formation. In this case, the tryptophan environment of both partners was unchanged upon interaction.

■ DISCUSSION

Enolase is an enzyme that plays a central role in the carbon metabolism of most organisms by participating in glycolysis and gluconeogenesis. Enolase also participates in a variety of functions and has multiple locations either inside or outside cells. The functions might include transport,[35] cell adhesion,[36] actin cytoskeleton remodeling,[37] and plasminogen receptor[18,19,38,39] among many other options, depending on the biological species. Nevertheless, it is not fully established whether the moonlighting functions of enolase are evolutionarily conserved. Neither the structure nor the oligomeric state necessary to perform each function is well defined. The physiological environment in which enolase is found may play an important role in its oligomeric state and consequently in its function.[5] Therefore, this protein has become an important target for drug and vaccine designs, to fight either infections caused by bacteria[40] or parasites,[41] or cancer,[42–44] and even to cure diabetes.[45,46] Therefore, describing the structure, the oligomeric state, and the mechanisms or conditions for self-association, which might be related to stability, multifunctionality, and trafficking within the cell among other characteristics of this protein, offers additional perspectives for both drug discovery and vaccination. Particularly, for enolases from *T. vaginalis*, this information has relevance due to the special sequence characteristics of these proteins, including the three key substitutions within one of the loops of the active site, compared to those of the human host enolase, as well as the unique N-terminal motif, composed of 15–18 residues, observed in enolases from the parasite.[19]

The ability of enolases from several biological species to self-associate and dissociate into monomers has been the subject of several studies.[47–54] In some cases, enolase can be detected merely in its dimeric state under native conditions[55,56] and monomers can be obtained by submitting the enzyme to chaotropic agents, such as temperature and hydrostatic pressure, and chemical agents, such as sodium perchlorate, or imidazole.[47–54] Whether or not the monomer of enolase has enzymatic activity depends on the biological origin of the enzyme and the conditions of dissociation. Additionally, some enolases can populate only the octameric state[15] but mixtures of oligomeric-state species have also been reported.[14] For example, the octameric enolase from *S. pyogenes* could be dissociated into monomers but dimers could not be produced, nor could any other oligomeric state.[14]

Here, we found three oligomeric-state species of a recombinant construct of enolase from *T. vaginalis* (TvEnoΔ34) coexisting in solution under nonharsh physicochemical conditions by changing the buffer solution in which enolase is diluted. The relative population of the species depends, as expected, on protein concentration. Indeed, higher protein concentrations enable higher oligomeric states but it seems that the cosolute type (potassium phosphate, Tris–acetate, Tris–HCl, and Mg^{2+}) has a stronger influence in determining the percentages of monomers, dimers, and octamers in solution. A single oligomeric species of TvEnoΔ34 could not be isolated under our experimental conditions, even by attempts using gel-filtration chromatography. The mixtures of species obtained do not show enzymatic activity, probably due to slight conformational changes involving both secondary and tertiary structures upon changing the buffer solution. In contrast, all combinations of oligomeric species show the ability to bind human plasminogen. According to 3D models of all three oligomeric species (monomer, dimer, and octamer), enolase should be prone to bind plasminogen by exposing the amino acid residues of the widely accepted putative plasminogen-binding motif ([264]FYDEEKKLY[272]) to the surface (Figures 3 and S3). It has been described that the enolase–plasminogen complex is formed by non-native conformations of the partners.[55,56] Conformations achieved in potassium phosphate, Tris–HCl, and Tris–acetate buffers might lose their nativeness to have enzymatic activity but are perturbed enough to be capable of binding plasminogen. The affinity toward plasminogen is variable and depends on the conformation of mixtures, but in all cases, either the hydrophobic environment of tryptophans or the secondary structure, or both are modified upon interaction. Additionally, the thermal stability of the combinations is variable. Remarkably, the unfolded state attained in the presence of phosphate ions maintains an important amount of secondary structure since the CD signal of the profiles under these conditions does not vary substantially. As expected, Mg^{2+} stabilizes TvEnoΔ34, probably by enabling higher-order oligomeric states.

T. vaginalis is a very primitive parasite with a large genetic multiplicity that[57,58] provides the parasite the ability to respond to drastic environmental changes (such as temperature, microflora, pH, iron concentration, polyamines, zinc, host immune responses, and other unknown factors) by modulating the expression of multiple genes. In *T. vaginalis*, there are nine genes encoding enolase. Here, we found that the product of the gene TVAG_329460, which was described as a plasminogen receptor, is capable of forming several oligomeric states in equilibrium under nonharsh conditions. This is not the first time that glycolytic enzymes from *T. vaginalis* have

shown distinctive self-association characteristics compared with their orthologs from other biological species. An interesting example corresponds to triose phosphate isomerase (TvTIM). In *T. vaginalis*, there are two isoforms of this enzyme (TvTIM1 and TvTIM2), which differ by four amino acids in their protein sequences. They share enzymatic parameters and overall scaffolds, but they display substantial differences in their stabilities. TvTIM1 is more stable and less dissociable than TvTIM2. The differences in sequence and mainly in stability provide alternative functions to a TIM barrel protein as a laminin- and fibronectin-binding protein.[59−61] This is one of the simplest examples of functional differentiation upon mutation.

■ CONCLUDING REMARKS

Monomers, dimers, and octamers of enolase from *T. vaginalis* coexist in solution in a variety of mild experimental conditions. As expected, the oligomeric state depends strongly on the protein concentration but it is not the main variable, dictating the self-association of enolase from *T. vaginalis*. The cosolute (buffer-salt and cofactor) importantly determines the dynamic self-association equilibria of TvEno.

Nevertheless, important questions must be addressed. How does a cosolute participate in the formation of different oligomeric states? Do different oligomeric states coexist within the cell? Which is the series of events taking place to adopt different oligomeric states? Are the mixtures capable of performing alternative functions of this protein? Is the oligomeric state of TvEno a type of function-regulation mechanism? Does the quaternary structure define the moonlighting function of enolase? All of these questions should be addressed with further investigation.

■ MATERIALS AND METHODS

Purification of Enolase. The gene identified as TVAG_329460 (UniProt entry A2EBB4) was amplified from genomic DNA of *T. vaginalis*. The polymerase chain reaction (PCR) primers were 5′-aac ggg aat cat atg aag gct ctc atc gag aag gtt g-3′ (forward) and 5′-gag gac gga tcctta ttc ctc agc gag cat gtc-3′ (reverse). Using these primers, the amplified sequence corresponds to an N-terminal-truncated version of enolase, eliminating 34 amino acid residues; therefore, the protein construct is depicted as TvEnoΔ34 (Figure S3). The PCR product was cloned into the *NdeI* and *BamHI* restriction sites (underlined) of a modified pET19 vector (courtesy of Professor Tom Ellenberger, Washington University School of Medicine). The plasmid pET19:TVAG_329460Δ34 was used to transform the Rosetta II strain of *Escherichia coli*. Cultures were grown to an optical density of 0.6 (600 nm) in 2xYT medium (plus 100 μg L^{-1} ampicillin and 34 μg L^{-1} chloramphenicol) at 37 °C. TvEnoΔ34 protein expression and purification were performed as described earlier.[19] Protein homogeneity was analyzed by sodium dodecyl sulfate-polyacrylamide gel electrophoresis (12%). After purification, enolase was extensively dialyzed against each buffer used: Tris−HCl, Tris−acetate, or potassium phosphate at 50 mM and pH 8.0 and stored at 4 °C for no more than 2 weeks.

Enzymatic Activity. The coupled reactions of rabbit muscle pyruvate kinase (PYK) and beef heart lactate dehydrogenase (LDH) were used to test enolase activity by following the decrease of NADH absorbance at 340 nm using a Scinco S-3100 UV−vis spectrophotometer. Standard activity assays were performed at 25 °C in a 1.0 mL reaction mixture containing 100 mM triethanolamine HCl, pH 7.4; 1.9 mM 2-PGA; 1.3 mM ADP; 0.12 mM β-NADH; 2 mM MgSO$_4$, and 100 mM KCl. The auxiliary enzymes PYK and LDH were used at final activities of 7 and 10 U mL^{-1}, respectively, and were purchased from Sigma. Recombinant enolase TvEnoΔ34 was added at a final concentration of 6.5 μg mL^{-1}. One activity unit is defined as the conversion of 1 μmol of substrate per min. The Michaelis constant (K_M) of enolase for 2-PGA was determined using the abovementioned reaction conditions by varying the concentration of 2-PGA between 1.9 nM and 1.9 mM.[8] Kinetic parameters were calculated from Michaelis−Menten plots by curve-fitting of experimentally determined data using the Origin program. Positive control experiments were performed using 0.025−0.05 units of commercial enolase from *S. cerevisiae* (ScEno), purchased from Sigma, without any further purification.

Homology Modeling of Different Oligomeric States of Recombinant Enolase from *T. vaginalis*. The 3D models of enolase from *T. vaginalis* of monomer, dimer, and octameric conformations were obtained using the SWISS-MODEL server (https://swissmodel.expasy.org/interactive).[20] Modeling templates were searched by using BLAST. The atomic coordinates of *S. pneumoniae* enolase were retrieved from the Protein Data Bank (PDB ID: 1W6T[21]). PyMOL program (The PyMOL Molecular Graphics System, Version 2.0 Schrödinger, LLC) was used to identify plasminogen-binding sites and tryptophan residues of each conformation.

CD Spectroscopy and Thermal Denaturation Transitions Were Monitored. CD measurements were performed in a JASCO J-815 spectropolarimeter (Jasco Inc., Easton, MD) equipped with a PFD-425S Peltier-type cell holder for temperature control and magnetic stirring. CD spectra were recorded from 200 to 250 nm using 1.0 cm path length cells. Ellipticities are reported as the mean residue ellipticity. Thermal denaturation transitions were followed by continuous monitoring of changes in ellipticity at a fixed wavelength of 220 nm, whereas the temperature of the sample was increased at a constant heating rate (2 °C min^{-1}). Actual temperatures within the cell were registered with the external cell holder probe. Cooling profiles were recorded after denaturation transitions had been completed. The temperature of heating and cooling profiles was registered and controlled through the Peltier accessory.

Fluorescence. Fluorescence spectra were obtained using an LS-55 Spectrofluorometer (PerkinElmer) equipped with a water-jacketed cell holder for controlling the temperature at 25 °C. The path length of quartz cuvettes was 1.0 cm. Spectra were recorded using two excitation wavelengths, 280 and 295 nm (as stated), and the emission spectra were collected from 320 to 400 nm and from 335 to 450 nm, respectively. The spectral center of mass (SCM) was calculated using the following equation

$$\text{SCM} = \sum (\lambda \times I_\lambda) / \sum I_\lambda \tag{1}$$

where I_λ represents the intensity data at each wavelength (λ) in the interval recorded.[22]

Small-Angle X-ray Scattering (SAXS). Small-angle X-ray scattering (SAXS) experiments were carried out by means of a Kratky camera coupled to a copper anode X-ray tube whose Kα radiation was selected with a nickel filter. The samples were introduced into a capillary tube. The SAXS intensity data, $I(q)$,

were collected with a linear proportional counter at a distance of 25 cm from the sample. In each case, the corresponding background was subtracted. Afterward, the data were processed with ITP program.[23−27] The momentum transfer or scattering vector is defined as $h = (4\pi \sin\theta)/\lambda$, where 2θ is the scattering angle and λ is the beam wavelength. The shapes of the particles were determined by the shape of the Kratky curve,[25] and the size distributions of the particles were calculated.

Interaction with Plasminogen. The evaluation of plasminogen binding was tested by differential far-UV-CD and intrinsic fluorescence spectroscopies. Plasminogen human plasma was purchased from Sigma and used without any further purification at a molar concentration equivalent to the enolase concentration in terms of a monomer. The buffers used and experimental parameters were the same as stated above.

ASSOCIATED CONTENT

ⓈSupporting Information

The Supporting Information is available free of charge on the ACS Publications website at DOI: 10.1021/acsome-ga.8b02197.

> Representative Kratky plots and (B) size distribution function of enolase diluted in Tris−HCl buffer at a concentration of 300 μg mL^{-1} (Figure S1); intrinsic fluorescence-emission spectra (excitation wavelength 280 and 295 nm) of native recombinant enolase TvEnoΔ34 (Figure S2); sequence of TvEnoΔ34 from *T. vaginalis*, predicted secondary structures are indicated (Figure S3); far-UV circular dichroism and intrinsic fluorescence-emission (excitation wavelength 295 nm) spectra of native human plasminogen, demonstrating different secondary and tertiary structure (Figure S4) (PDF)

AUTHOR INFORMATION

Corresponding Author
*E-mail: beni1972uk@gmail.com.

ORCID Ⓞ
Elibeth Mirasol-Meléndez: 0000-0001-8308-7161

Notes
The authors declare no competing financial interest.
Authors attest that this article is original and they agree with the publication of the manuscript without any ethical issues involved.

ACKNOWLEDGMENTS

REFERENCES

(1) Brewer, J. M. Yeast enolase: mechanism of activation by metal ions. *Crit. Rev. Biochem.* **1981**, *11*, 209−254.

(2) Ji, H.; et al. Progress in the biological function of alpha-enolase. *Anim. Nutr.* **2016**, *2*, 12−17.

(3) Funk, J.; Schaarschmidt, B.; Slesiona, S.; Hallström, T.; Horn, U.; Brock, M. The glycolytic enzyme enolase represents a plasminogen-binding protein on the surface of a wide variety of medically important fungal species. *Int. J. Med. Microbiol.* **2016**, *306*, 59−68.

(4) Nogueira, S. V.; Smith, A. A.; Qin, J.-H.; Pal, U. A surface enolase participates in *Borrelia burgdorferi*-plasminogen interaction and contributes to pathogen survival within feeding ticks. *Infect. Immun.* **2012**, *80*, 82−90.

(5) Paludo, G. P.; Lorenzatto, K. R.; Bonatto, D.; Ferreira, H. B. Systems biology approach reveals possible evolutionarily conserved moonlighting functions for enolase. *Comput. Biol. Chem.* **2015**, *58*, 1−8.

(6) Díaz-Ramos, À.; Roig-Borrellas, A.; García-Melero, A.; López-Alemany, R. α-Enolase, a multifunctional protein: its role on pathophysiological situations. *J. Biomed. Biotechnol.* **2012**, *2012*, No. 156795.

(7) Brewer, J. M.; Glover, C. V.; Holland, M. J.; Lebioda, L. Effect of site-directed mutagenesis of His373 of yeast enolase on some of its physical and enzymatic properties. *Biochim. Biophys. Acta* **1997**, *1340*, 88−96.

(8) Hannaert, V.; et al. Kinetic characterization, structure modelling studies and crystallization of *Trypanosoma brucei* enolase. *Eur. J. Biochem.* **2003**, *270*, 3205−3213.

(9) Stec, B.; Lebioda, L. Refined structure of yeast apo-enolase at 2.25 A resolution. *J. Mol. Biol.* **1990**, *211*, 235−248.

(10) Lu, Q.; Lu, H.; Qi, J.; Lu, G.; Gao, G. F. An octamer of enolase from *Streptococcus suis*. *Protein Cell* **2012**, *3*, 769−780.

(11) Wu, Y.; et al. Octameric structure of *Staphylococcus aureus* enolase in complex with phosphoenolpyruvate. *Acta Crystallogr., Sect. D: Biol. Crystallogr.* **2015**, *71*, 2457−2470.

(12) Kolberg, J.; et al. *Streptococcus pneumoniae* enolase is important for plasminogen binding despite low abundance of enolase protein on the bacterial cell surface. *Microbiology* **2006**, *152*, 1307−1317.

(13) Brown, C. K.; Kuhlman, P. L.; Mattingly, S.; Slates, K.; Calie, P. J.; Farrar, W. W. A model of the quaternary structure of enolases, based on structural and evolutionary analysis of the octameric enolase from *Bacillus subtilis*. *J. Protein Chem.* **1998**, *17*, 855−866.

(14) Karbassi, F.; Quiros, V.; Pancholi, V.; Kornblatt, M. J. Dissociation of the Octameric Enolase from *S. pyogenes* - One Interface Stabilizes Another. *PLoS One* **2010**, *5*, No. e8810.

(15) Lu, Q.; Lu, H.; Qi, J.; Lu, G.; Gao, G. F. An octamer of enolase from *Streptococcus suis*. *Protein Cell* **2012**, *3*, 769−780.

(16) Arbabi, M.; Delavari, M.; Fakhrieh-Kashan, Z.; Hooshyar, H. Review of *Trichomonas vaginalis* in Iran, Based on Epidemiological Situation. *J. Reprod. Infertil.* **2018**, *19*, 82−88.

(17) Aurrecoechea, C.; et al. GiardiaDB and TrichDB: integrated genomic resources for the eukaryotic protist pathogens *Giardia lamblia* and *Trichomonas vaginalis*. *Nucleic Acids Res.* **2009**, *37*, D526−D530.

(18) Mundodi, V.; Kucknoor, A. S.; Alderete, J. F. Immunogenic and plasminogen-binding surface-associated alpha-enolase of *Trichomonas vaginalis*. *Infect. Immun.* **2008**, *76*, 523−531.

(19) Mirasol-Meléndez, E.; et al. Characterization of multiple enolase genes from *Trichomonas vaginalis*. Potential novel targets for drug and vaccine design. *Parasitol. Int.* **2018**, *67*, 444−453.

(20) Biasini, M.; et al. SWISS-MODEL: modelling protein tertiary and quaternary structure using evolutionary information. *Nucleic Acids Res.* **2014**, *42*, W252−W258.

(21) Ehinger, S.; Schubert, W.-D.; Bergmann, S.; Hammerschmidt, S.; Heinz, D. W. Plasmin(ogen)-binding alpha-enolase from *Streptococcus pneumoniae*: crystal structure and evaluation of plasmin-(ogen)-binding sites. *J. Mol. Biol.* **2004**, *343*, 997−1005.

(22) Nájera, H.; Costas, M.; Fernández-Velasco, D. A. Thermodynamic characterization of yeast triosephosphate isomerase refolding: insights into the interplay between function and stability as reasons for the oligomeric nature of the enzyme. *Biochem. J.* **2003**, *370*, 785−792.

(23) Glatter, O. Convolution square root of band-limited symmetrical functions and its application to small-angle scattering data. *J. Appl. Crystallogr.* **1981**, *14*, 101−108.

(24) Walenta, E. Small angle x-ray scattering. Von O. GLATTER und O. KRATKY. London: Academic Press Inc. Ltd. 1982. ISBN 0-12-286280-5. X, 515 Seiten, geb. £ 43,60; US $; 81.00. *Acta Polym.* **1985**, *36*, 296.

(25) Glatter, O.; Sieberer, J.; Schnablegger, H. A Comparative Study on Different Scattering Techniques and data evaluation methods for sizing of colloidal systems using light scattering. *Part. Part. Syst. Charact.* **1991**, *8*, 274−281.

(26) Glatter, O.; Hofer, M. Elastic light scattering from nonspherical and polydisperse particles in the size range from 100 to 2000 NM. *Makromol. Chem., Macromol. Symp.* **1988**, *15*, 191−200.

(27) Glatter, O.; Hainisch, B. Improvements in real-space deconvolution of small-angle scattering data. *J. Appl. Crystallogr.* **1984**, *17*, 435−441.

(28) Korasick, D. A.; Tanner, J. J. Determination of protein oligomeric structure from small-angle X-ray scattering. *Protein Sci.* **2018**, *27*, 814−824.

(29) Moreno-Vargas, L. M.; Carrillo-Ibarra, N.; Arzeta-Pino, L.; Benítez-Cardoza, C. G. Thermal unfolding of apo- and holo-enolase from *Saccharomyces cerevisiae*: different mechanisms, similar activation enthalpies. *Int. J. Biol. Macromol.* **2011**, *49*, 871−878.

(30) McCorvie, T. J.; Liu, Y.; Frazer, A.; Gleason, T. J.; Fridovich-Keil, J. L.; Timson, D. J. Altered cofactor binding affects stability and activity of human UDP-galactose 4′-epimerase: implications for type III galactosemia. *Biochim. Biophys. Acta* **2012**, *1822*, 1516−1526.

(31) Risse, B.; Stempfer, G.; Rudolph, R.; Schumacher, G.; Jaenicke, R. Characterization of the stabilizing effect of point mutations of pyruvate oxidase from *Lactobacillus plantarum*: Protection of the native state by modulating coenzyme binding and subunit interaction. *Protein Sci.* **1992**, *1*, 1710−1718.

(32) Michel, B.; Proudfoot, A. E.; Wallace, C. J.; Bosshard, H. R. The cytochrome c oxidase-cytochrome c complex: spectroscopic analysis of conformational changes in the protein-protein interaction domain. *Biochemistry* **1989**, *28*, 456−462.

(33) Bothner, B.; Lewis, W. S.; DiGiammarino, E. L.; Weber, J. D.; Bothner, S. J.; Kriwacki, R. W. Defining the molecular basis of Arf and Hdm2 interactions11Edited by F. Cohen. *J. Mol. Biol.* **2001**, *314*, 263−277.

(34) Greenfield, N. J. Circular dichroism (CD) analyses of protein-protein interactions. *Methods Mol. Biol.* **2015**, *1278*, 239−265.

(35) Decker, B. L.; Wickner, W. T. Enolase Activates Homotypic Vacuole Fusion and Protein Transport to the Vacuole in Yeast. *J. Biol. Chem.* **2006**, *281*, 14523−14528.

(36) Kinoshita, H.; Ohuchi, S.; Arakawa, K.; Watanabe, M.; Kitazawa, H.; Saito, T. Isolation of lactic acid bacteria bound to the porcine intestinal mucosa and an analysis of their moonlighting adhesins. *Biosci. Microbiota, Food Health* **2016**, *35*, 185−196.

(37) Vizin, T.; Kos, J. Gamma-enolase: a well-known tumour marker, with a less-known role in cancer. *Radiol. Oncol.* **2015**, *49*, 217−226.

(38) Ayón-Núñez, D. A.; et al. Identification and characterization of *Taenia solium* enolase as a plasminogen-binding protein. *Acta Trop.* **2018**, *182*, 69−79.

(39) Cork, A. J.; et al. Stability of the Octameric Structure Affects Plasminogen-Binding Capacity of Streptococcal Enolase. *PLoS One* **2015**, *10*, No. e0121764.

(40) Chen, S.; Liu, Y.; Zhang, J.; Gao, B. iTRAQ-based quantitative proteomic analysis of *Microcystis aeruginosa* exposed to spiramycin at different nutrient levels. *Aquat. Toxicol.* **2017**, *185*, 193−200.

(41) Avilán, L.; et al. Enolase: A Key Player in the Metabolism and a Probable Virulence Factor of Trypanosomatid Parasites—Perspectives for Its Use as a Therapeutic Target. *Enzyme Res.* **2011**, *2011*, No. 932549.

(42) Wang, L.; et al. A novel α-enolase-targeted drug delivery system for high efficacy prostate cancer therapy. *Nanoscale* **2018**, *10*, 13673−13683.

(43) Su, S.; et al. CS5931, a novel marine polypeptide, inhibits migration and invasion of cancer cells via interacting with enolase 1. *Recent Pat. Anti-Cancer Drug Discovery* **2018**, *13*, 360−367.

(44) Wu, C.-H.; Kuo, Y.-H.; Hong, R.-L.; Wu, H.-C. α-Enolase-binding peptide enhances drug delivery efficiency and therapeutic efficacy against colorectal cancer. *Sci. Transl. Med.* **2015**, *7*, No. 290ra91.

(45) Cho, H.; et al. ENOblock, a unique small molecule inhibitor of the non-glycolytic functions of enolase, alleviates the symptoms of type 2 diabetes. *Sci. Rep.* **2017**, *7*, No. 44186.

(46) Satani, N.; Lin, Y.-H.; Hammoudi, N.; Raghavan, S.; Georgiou, D. K.; Muller, F. L. ENOblock Does Not Inhibit the Activity of the Glycolytic Enzyme Enolase. *PLoS One* **2016**, *11*, No. e0168739.

(47) Pal-Bhowmick, I.; Krishnan, S.; Jarori, G. K. Differential susceptibility of *Plasmodium falciparum* versus yeast and mammalian enolases to dissociation into active monomers. *FEBS J.* **2007**, *274*, 1932−1945.

(48) Kornblatt, M. J.; Hoa, G. H. B. The pressure-induced inactivation of mammalian enolases is accompanied by dissociation of the dimeric enzyme. *Arch. Biochem. Biophys.* **1987**, *252*, 277−283.

(49) Trepanier, D.; Wong, C.; Kornblatt, M. J. The salt-induced dissociation and inactivation of a mammalian enolase: evidence for the formation of active monomers. *Arch. Biochem. Biophys.* **1990**, *283*, 271−277.

(50) Kornblatt, M. J.; Kornblatt, J. A.; Hoa, G. H. B. The role of water in the dissociation of enolase, a dimeric enzyme. *Arch. Biochem. Biophys.* **1993**, *306*, 495−500.

(51) Kornblatt, M. J.; Al-Ghanim, A.; Kornblatt, J. A. The effects of sodium perchlorate on rabbit muscle enolase–Spectral characterization of the monomer. *Eur. J. Biochem.* **1996**, *236*, 78−84.

(52) Kornblatt, M. J.; Lange, R.; Balny, C. Can monomers of yeast enolase have enzymatic activity? *Eur. J. Biochem.* **1998**, *251*, 775−780.

(53) Kornblatt, M. J.; Lange, R.; Balny, C. Use of hydrostatic pressure to produce 'native' monomers of yeast enolase. *Eur. J. Biochem.* **2004**, *271*, 3897−3904.

(54) Vora, H. K.; Shaik, F. R.; Pal-Bhowmick, I.; Mout, R.; Jarori, G. K. Effect of deletion of a plant like pentapeptide insert on kinetic, structural and immunological properties of enolase from *Plasmodium falciparum*. *Arch. Biochem. Biophys.* **2009**, *485*, 128−138.

(55) Kornblatt, M. J.; Kornblatt, J. A.; Hancock, M. A. The interaction of canine plasminogen with *Streptococcus pyogenes* enolase: they bind to one another but what is the nature of the structures involved? *PLoS One* **2011**, *6*, No. e28481.

(56) Balhara, V.; Deshmukh, S. S.; Kálmán, L.; Kornblatt, J. A. The interaction of streptococcal enolase with canine plasminogen: the role of surfaces in complex formation. *PLoS One* **2014**, *9*, No. e88395.

(57) Leitsch, D. Recent Advances in the *Trichomonas vaginalis* Field. *F1000Research* **2016**, *5*, 162.

(58) Mielczarek, E.; Blaszkowska, J. *Trichomonas vaginalis*: pathogenicity and potential role in human reproductive failure. *Infection* **2016**, *44*, 447−58.

(59) Lara-González, S.; et al. Structural and thermodynamic folding characterization of triosephosphate isomerases from *Trichomonas vaginalis* reveals the role of destabilizing mutations following gene duplication. *Proteins: Struct., Funct., Bioinf.* **2014**, *82*, 22−33.

(60) Lara-Gonzalez, S.; et al. Substrate-Induced Dimerization of Engineered Monomeric Variants of Triosephosphate Isomerase from *Trichomonas vaginalis*. *PLoS One* **2015**, *10*, No. e0141747.

(61) Miranda-Ozuna, J. F. T.; et al. The Glycolytic Enzyme Triosephosphate Isomerase of *Trichomonas vaginalis* Is a Surface-Associated Protein Induced by Glucose That Functions as a Laminin- and Fibronectin-Binding Protein. *Infect. Immun.* **2016**, *84*, 2878−2894.